Figure 1

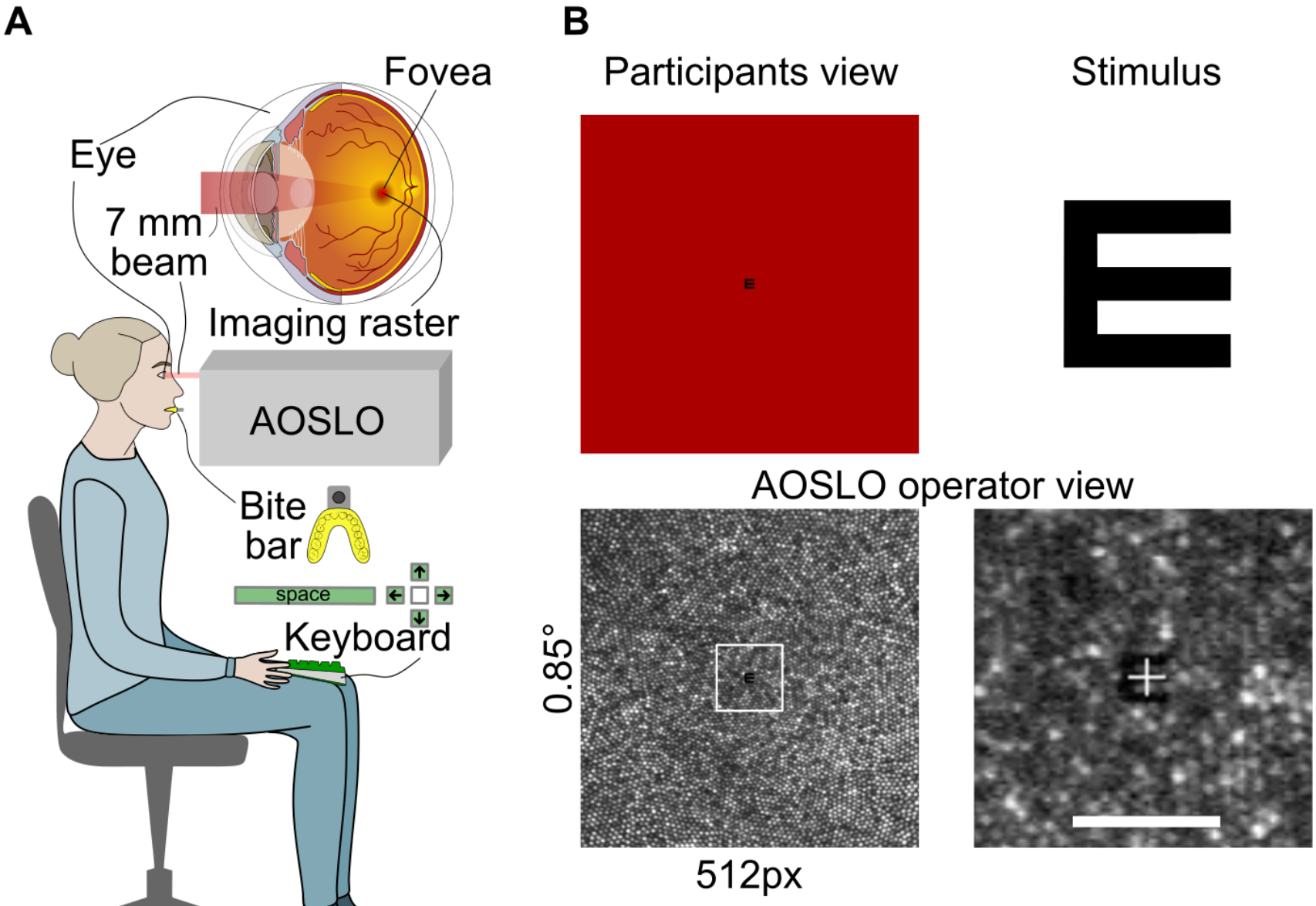
A
Fovea
Eye
7 mm
beam
Imaging raster
AOSLO
Bite
bar
space
Keyboard
B
Participants view
Stimulus
AOSLO operator view
0.85°
512px

Figure 2

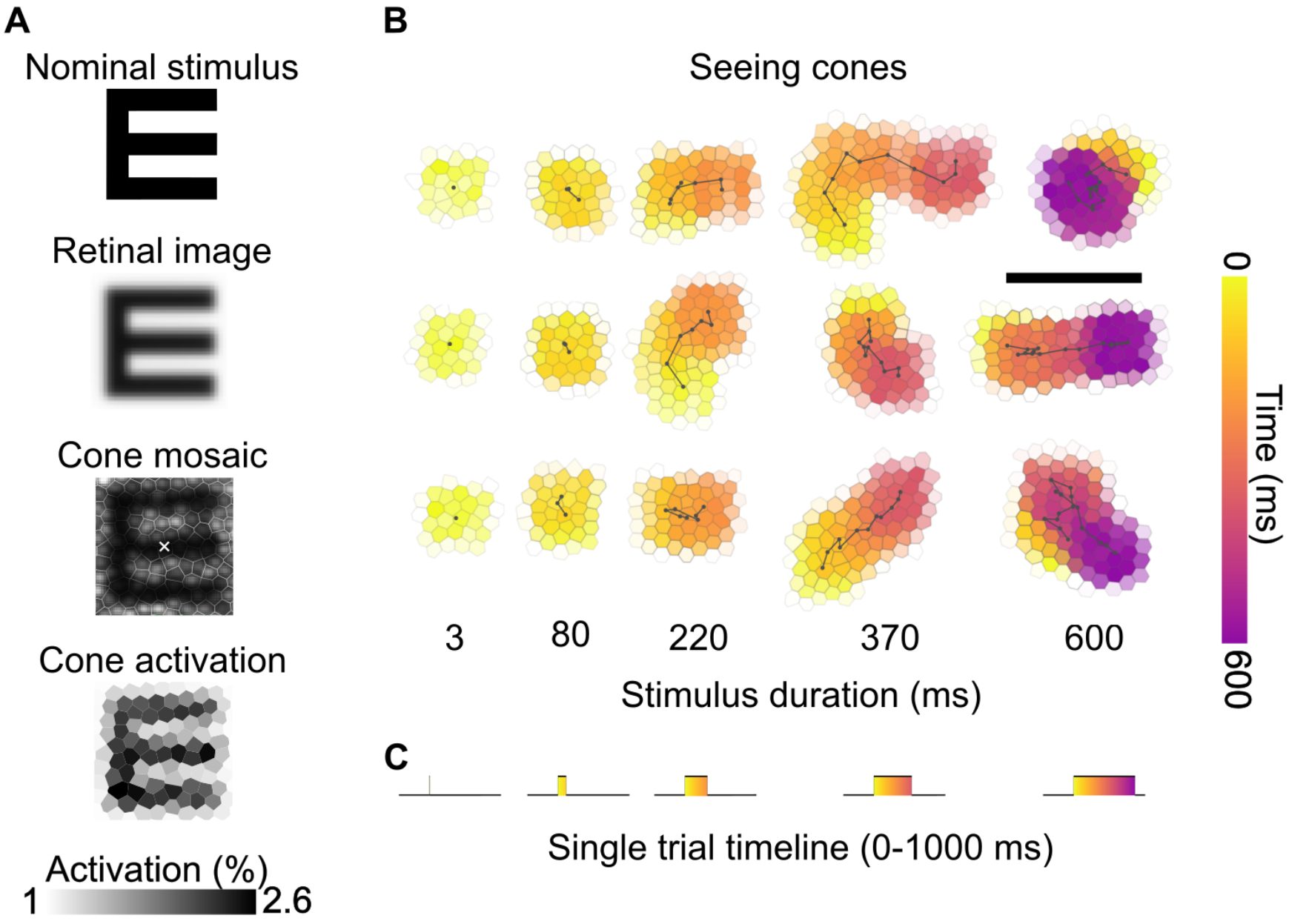
A
Nominal stimulus
Retinal image
Cone mosaic
Cone activation
Activation (%)
1
2.6
B
Seeing cones
3
80
220
370
600
Stimulus duration (ms)
Time (ms)
0
600
C
Single trial timeline (0-1000 ms)

Figure 3

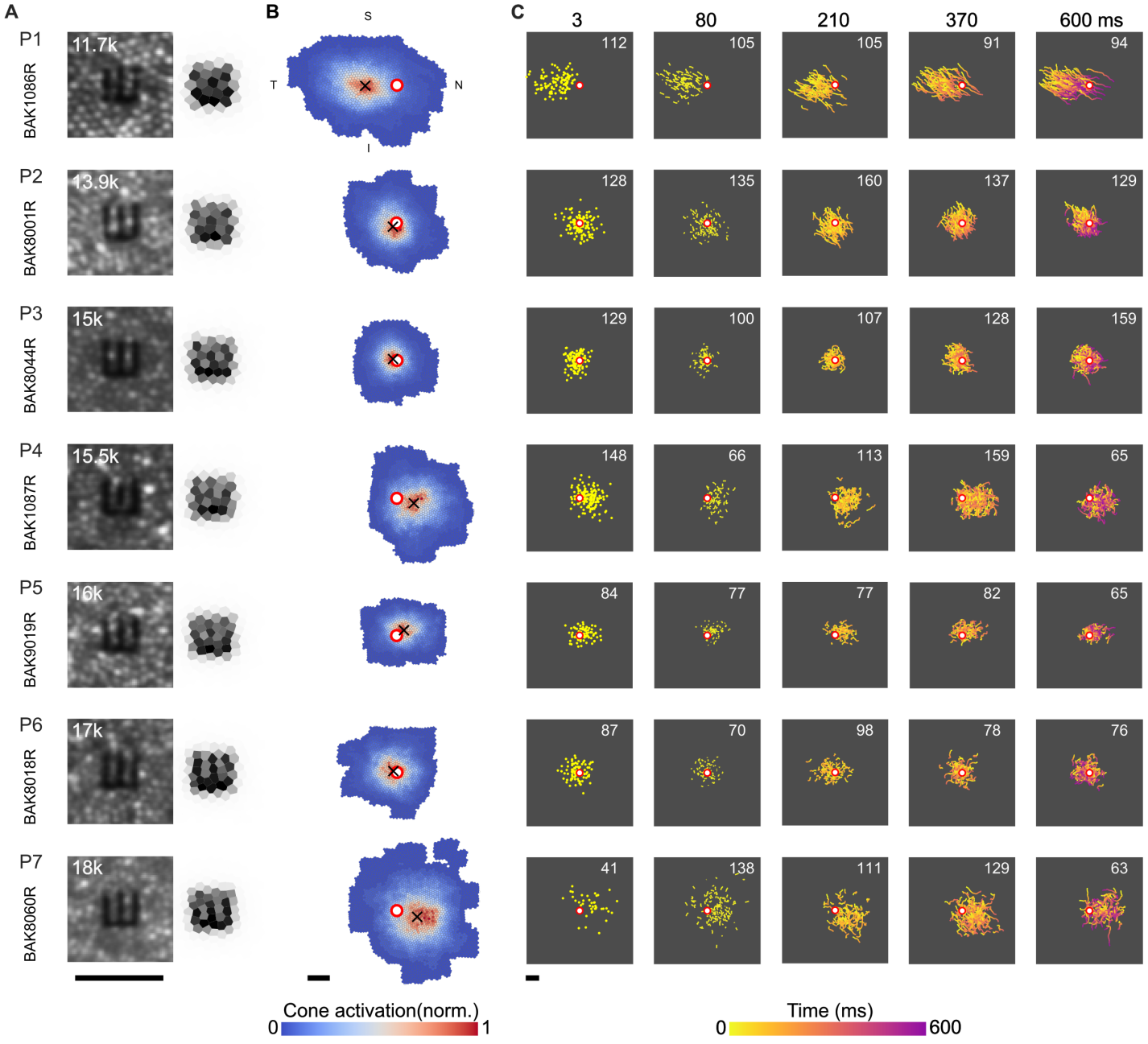
A
B
C
S
T
N
I
3
80
210
370
600 ms
P1
BAK1086R
11.7k
112
105
105
91
94
P2
BAK8001R
13.9k
128
135
160
137
129
P3
BAK8044R
15k
129
100
107
128
159
P4
BAK1087R
15.5k
148
66
113
159
65
P5
BAK9019R
16k
84
77
77
82
65
P6
BAK8018R
17k
87
70
98
78
76
P7
BAK8060R
18k
41
138
111
129
63
Cone activation(norm.)
0
1
Time (ms)
0
600

Figure 4

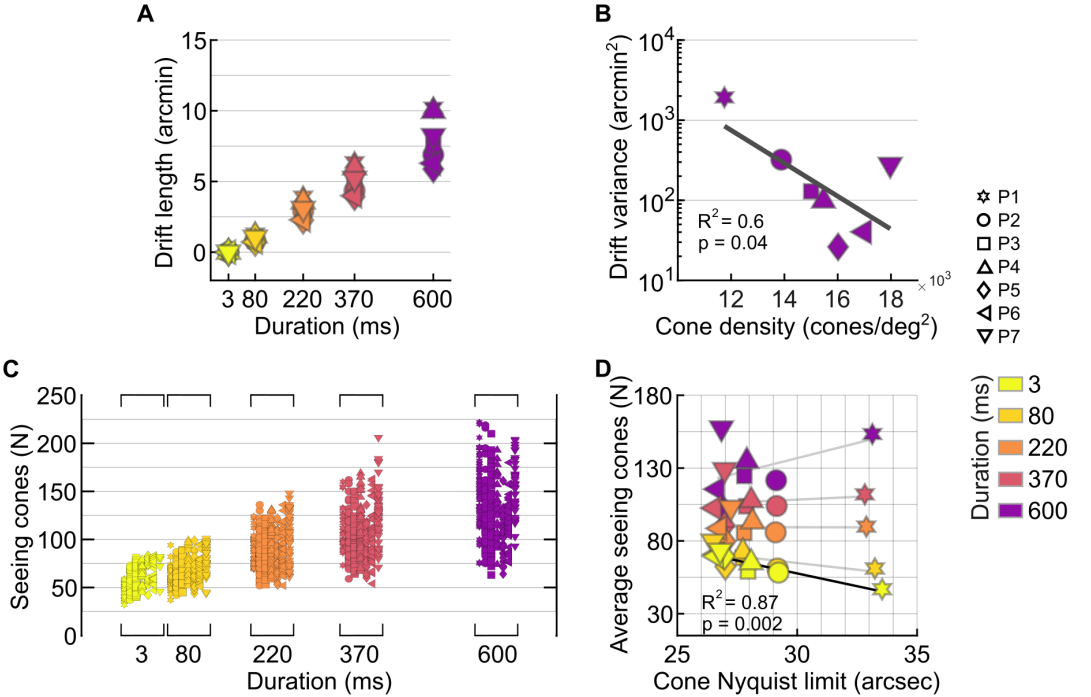
A
Drift length (arcmin)
15
10
5
0
3 80 220 370 600
Duration (ms)
B
Drift variance (arcmin²)
10⁴
10³
10²
10¹
R² = 0.6
p = 0.04
12 14 16 18
×10³
Cone density (cones/deg²)
P1
P2
P3
P4
P5
P6
P7
C
Seeing cones (N)
250
200
150
100
50
0
3 80 220 370 600
Duration (ms)
D
Average seeing cones (N)
180
130
80
30
R² = 0.87
p = 0.002
25 30 35
Cone Nyquist limit (arcsec)
Duration (ms)
3
80
220
370
600

Figure 5

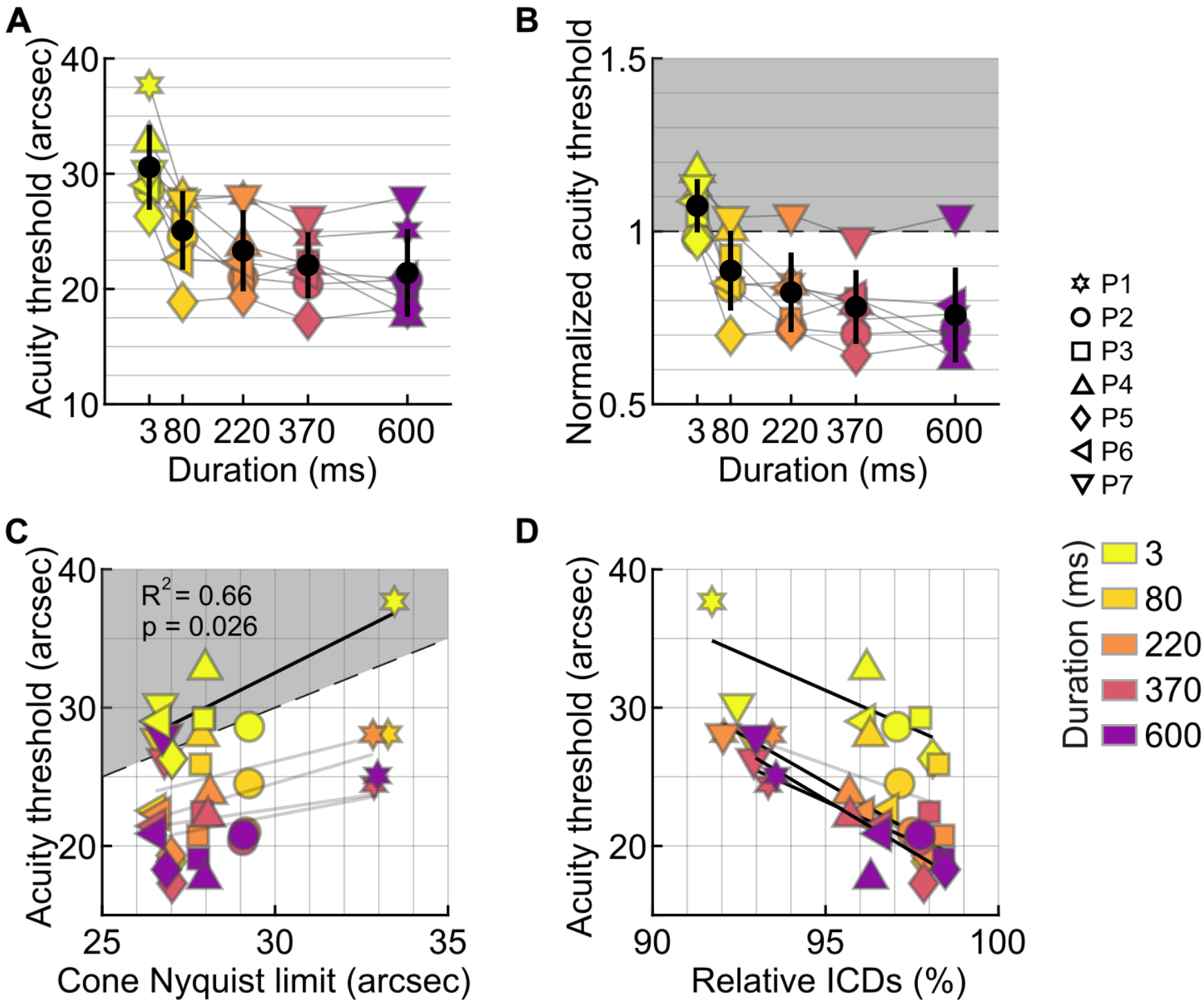
A
Acuity threshold (arcsec)
40
30
20
10
3 80 220 370 600
Duration (ms)
B
Normalized acuity threshold
1.5
1
0.5
3 80 220 370 600
Duration (ms)
P1
P2
P3
P4
P5
P6
P7
C
Acuity threshold (arcsec)
R^2 = 0.66
p = 0.026
40
30
20
25 30 35
Cone Nyquist limit (arcsec)
D
Acuity threshold (arcsec)
40
30
20
90 95 100
Relative ICDs (%)
Duration (ms)
3
80
220
370
600

Title: Sub-cone visual acuity can be achieved with less than 1 arcmin retinal slip

Authors: Veronika Lukyanova[1], Julius Ameln[1], Jenny L. Witten[1,2], Aleksandr Gutnikov[1], Maximilian Freiberg[1,3], Bilge Sayim[4], Wolf Harmening[1]

[1]Department of Ophthalmology, University of Bonn, Bonn, Germany

[2]Zeiss Vision Science Lab, Institute for Ophthalmic Research - Tübingen, Germany

[3]Berliner Hochschule für Technik, Berlin, Germany

[4]Laboratoire de Sciences Cognitives et Psycholinguistique (LSCP), Département d'Études Cognitives (DEC), École normale supérieure (ENS), UMR8554, Centre National de la Recherche Scientifique (CNRS), Paris, France

veronika.lukyanova@ukbonn.de,

julius.ameln@ukbonn.de,

jenny-loren.witten@zeiss.com,

aleksandr.gutnikov@ukbonn.de,

maximilian.freiberg@ukbonn.de,

bilge.sayim@ens.psl.eu

wolf.harmening@ukbonn.de

URL: https://ao.ukbonn.de

Abstract:

The retinal area inspecting a visual stimulus and, consequently, the number of photoreceptors engaged in a visual task, increases with presentation time, as fixational eye movements continuously move the retina across the retinal image. Here, we varied stimulus duration in a Tumbling-E visual acuity task while recording videos of the photoreceptor mosaic in seven participants with adaptive optics micro-psychophysical techniques, to determine how far the retinal image must move across the cone mosaic before this motion begins to improve visual acuity. Five stimulus presentation durations were tested (3, 80, 220, 370, and 600 ms), while participants exhibited natural eye movements. Retinal slip amplitudes, i.e. the total displacement stimuli underwent, increased linearly with stimulus duration at individual rates. Higher cone density was associated with drift over smaller retinal areas, making the number of traversed cones more similar across participants at longer durations. At the

shortest presentation duration, retinal slip was virtually absent and acuity was limited by retinal resolution, averaging to 1.07 ± 0.08 times the cone row-to-row spacing (Nyquist limit of sampling). At 80 ms duration, corresponding to approximately 2 cone diameters of retinal slip, acuity thresholds improved significantly, reaching 0.90 ± 0.1 of the Nyquist limit. Thresholds continued to improve with longer durations at a lower rate, reaching 0.75 ± 0.10 times the Nyquist limit at 600 ms. These results demonstrate that humans can extract visual information with sub-cone precision within less than 100 milliseconds with a retinal slip approaching single foveal cone spacing.

Keywords

foveal vision; adaptive optics; micro-psychophysics; fixational drift; cone photoreceptors.

Acknowledgments

Commercial relationships disclosure: V Lukyanova, None; Julius Ameln, None; Jenny L. Witten, Zeiss Vision Science Lab; Aleksandr Gutnikov, None; Bilge Sayim, None; W Harmening, None.

Funded by the Agence Nationale de la Recherche (ANR-19-FRAL-0004) and German Research Foundation (grants 430279747 and 548538462). This work was supported by the Open Access Publication Fund of the University of Bonn.

Corresponding author: Wolf M. Harmening

Use of generative AI-tools disclosure: During manuscript preparation, the authors used ChatGPT (OpenAI, GPT-4.5) to suggest minor grammar and wording edits on early drafts; any accepted edits were reviewed and revised by the authors, who take full responsibility for the final text.

Address: Rheinische Friedrich-Wilhelms-Universität Bonn, University Eye Hospital Bonn, Ernst-Abbe-Str. 2, 53127 Bonn, Germany.

Introduction

When humans fixate on a visual object, incessant fixational eye movements (FEM) translate retinal photoreceptors across the retinal image, dynamically updating visual sampling (Dodge, 1907; Yarbus, 1967; Martinez-Conde et al., 2004). This constant retinal slip creates a link between spatial sampling and the temporal exposure to a stimulus. One consequence is that more information is potentially yielded with longer fixation. Here we ask how many foveal cones a stimulus has to traverse to benefit visual acuity.

In the absence of any motion, our ability to resolve fine detail is theoretically limited by both the quality of the retinal image and by the sampling limit of the neural machinery (Campbell & Green, 1965; Westheimer, 2009). In the center of the foveola, the central 1-degree diameter of the retina, cone photoreceptor density is highest and the ascending visual pathways are built to preserve the cones' spatial grain (Walls, 1942; Polyak, 1957; Curcio & Allen, 1990; Tuten & Harmening, 2021). Under optimal optical conditions, when diffraction sets the upper bound to the quality of the retinal image, foveolar cone spacing dictates the highest resolvable spatial frequency before aliasing occurs (Westheimer & McKee, 1975; Williams, 1985). Thus, maximum visual resolution ought to be capped at the Nyquist limit of cone sampling, which equals the smallest row-to-row spacing of the foveal mosaic. By compensating for the eyes' natural aberrations with adaptive-optics corrected stimuli presented during natural FEM, however, visual acuity was shown to exceed this limit, reaching values as high as 20/8 vision, corresponding to spatial details that are 20 percent smaller than the Nyquist limit (Rossi et al., 2007; Witten et al., 2024). It is likely that the visual system leverages the temporal modulations in cone activity as produced by FEM to increase resolution beyond static sampling limits (Pitkow et al., 2007; Ahissar & Arieli, 2012; Nghiem et al., 2025).

Fixational drift, characterized by slow, small-amplitude movements, was show to be exploited by the visual brain in acuity tasks by its main feature – continuous motion – which leads to constant refresh of the visual input (Rucci & Poletti, 2015). Drift motion patterns are often described by random-walk statistics in theoretical models (Pitkow et al., 2007; Burak et al., 2010; Engbert et al., 2011;

Kuang et al., 2012; Anderson et al., 2020) and experimental research (Nachmias, 1961; Kuang et al., 2012; Intoy & Rucci, 2020; Clark et al., 2022; Ben-Shushan et al., 2022), but also as more structured, non-random patterns (Malevich et al., 2020; Hafed et al., 2021). This indicates that drift could not only be exploited but also controlled by the visual system in a favorable way, such as by moving retinal areas of higher cone density toward the object of interest (Witten et al., 2024). On a mechanistic level, drift may enhance acuity through optimal spatiotemporal flow of the retinal image either through sensor-derived temporal encoding (Ahissar & Arieli, 2001) or luminance modulations (Rucci & Victor, 2015). Moreover, the ongoing movement provides not just singular snapshots but multiple views of the retinal image (Ratnam et al., 2017; Anderson et al., 2020). At the same time, drift introduces spatial noise, posing a challenge that the visual system must compensate for (Packer & Williams, 1992; Murakami & Cavanagh, 1998, 2001; Pitkow et al., 2007; Burak et al., 2010). This might be achieved by neural stimulus tracking if minimal a priori knowledge of the stimulus is present (Nghiem et al., 2025).

Testing fixational drift as a mechanism that potentially aids acuity can be explored by varying the extent of retinal slip it produces. Such manipulation can be achieved by either retina-contingent stimulation (stabilization)(Ditchburn & Ginsborg, 1952; Riggs et al., 1953; Pritchard, 1961; Heckenmueller, 1965; Yarbus, 1967; Stevens et al., 1976; Kelly, 1979; Hammer et al., 2006; Arathorn et al., 2007), or by control of stimulus exposure duration (Riggs et al., 1953; Tulunay-Keesey & Jones, 1976). While early studies suggested better or no changes in performance under stabilization (Riggs et al., 1953; Keesey, 1960; Tulunay-Keesey & Jones, 1976; Kelly, 1979), more recent work using modern instrumentation indicates that external retinal stabilization degrades the perception of fine spatial detail (Rucci et al., 2007; Ratnam et al., 2017; Anderson et al., 2020; Intoy & Rucci, 2020). Experiments that manipulated presentation duration have shown that acuity generally improves with increasing stimulus exposure, plateauing after a few hundred milliseconds (Baron & Westheimer, 1973; Tulunay-Keesey & Jones, 1976; Alexander et al., 1993; Niwa & Tokoro, 1997; McAnany, 2014), or in some cases, continue to improve up to 10 seconds (Heinrich et al., 2010). Most psychophysical studies that measure acuity typically use stimulus

durations of 500 ms or longer to ensure saturated performance. During this time, the retinal image moves across a space equivalent to 30–50 foveal cone diameters (Rolfs, 2009; Ameln et al., 2025), an order of magnitude above the sampling limit. This leaves the minimal number of cones a stimulus must traverse to produce a measurable improvement in acuity not yet established by previous work.

Given the spatiotemporal interaction that FEM exerts on cone sampling, we investigated how visual acuity relates to stimulus duration, and asked what the minimum retinal slip is that produces a measurable benefit to visual acuity. To disentangle the contributions of retinal resolution and eye movement, we employed adaptive optics scanning light ophthalmoscopy (AOSLO). The AOSLO corrects the eye's higher-order optical aberrations (Roorda et al., 2002), produces cell-resolved images of the foveola with unambiguous landing positions of retinal stimuli (Reiniger et al., 2021), and allows precise tracking of retinal motion (Arathorn et al., 2007; Stevenson & Roorda, 2005). Thus, we ensured that any observed performance changes were driven by the interplay between FEM, stimulus duration and cone topography, rather than optical aberrations.

Methods

Participants

Seven human observers (three males and four females, mean age: 29.6, range: 19-44 years) with no known eye disease participated in the experiment. Written informed consent was obtained from all participants in accordance with the Declaration of Helsinki. The study was approved by the independent ethics committee of the Rheinische Friedrich-Wilhelms-Universität Bonn. General eye health was confirmed by an ophthalmologist. Pupils were dilated and accommodation was paralyzed by administration of two drops of 0.5% Tropicamide 15 minutes before the experimental session, with additional drops administered if necessary to ensure adequate mydriasis and cycloplegia throughout the experiments. Imaging and psychophysical testing was conducted in the dominant eye only, identified using the Miles Test prior to dilation (right eyes in all participants). Participants' refractive errors by means of spherical equivalent

ranged from plano to -1,0 diopter. To position and stabilize the head in front of the imaging instrument, a custom dental impression (bite bar) was made for each participant. Participant naming used throughout the analysis, P1-P7, followed an ascending order of their cone density at the anatomical center of the foveola, expressed in cones per square degree of visual angle.

AOSLO micro-psychophysics

For in-vivo retinal imaging and visual stimulation with foveal cone resolution, a custom-built adaptive optics scanning light ophthalmoscope (AOSLO) was used. Instrument details and micro-psychophysical procedures have been described before (Roorda et al., 2002; Domdei et al., 2021). In short, the AOSLO created an image of and a stimulus on the retina of the test eye by an intensity modulated point-scanned 788 nm light, spanning a square field on the retina of 0.85 × 0.85 degrees of visual angle (**Fig. 1**). Ocular aberrations were compensated by closed-loop adaptive optics correction, ensuring continuous diffraction-limited beam formation for both imaging and stimulation irrespective of experiment duration. The AOSLO creates videos from which the exact location and motion path of a retinal stimulus can be assessed with high temporal and sub-cellular spatial resolution by image registration techniques.

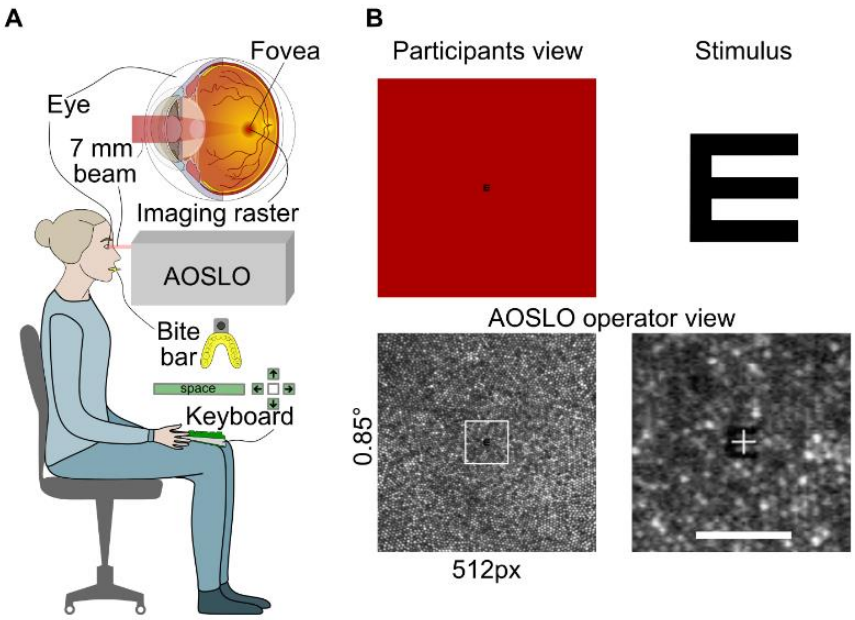

Figure 1. High-resolution AOSLO imaging and micropsychophysics.
(A) Schematic representation of the setup for foveal acuity testing with adaptive optics scanning laser

ophthalmoscopy (AOSLO). Participants sat upright in the AOSLO system, with head movements quelled by a custom-made bite bar. A 788 nm, 7 mm diameter beam was directed into the participant's eye, and scanned across a 0.85-degree field. Each trial was initiated by the participant pressing the spacebar on a keyboard placed on their lap, triggering the recording of a one-second AOSLO video. This followed by reporting the orientation of the tumbling-E stimulus using one of the arrow keys. (B) The Tumbling-E acuity stimulus, shown in the top-right panel, appeared in the center of the scanning raster (top-left). The AOSLO operator concurrently observed the retinal image, visualizing the participant's cone mosaic (lower left). The bottom-right panel shows a magnified view of a single AOSLO video frame with the stimulus visible at the center. Scale bar is 5 arcmin.

Prior to the first experimental sessions, a high-resolution foveal montage was created for each eye, similar as previously described (Ameln et al., 2025). At least three videos were recorded for ten fixation locations, including the center, corners, and midpoints of the imaging raster. Videos were stabilized offline using an improved strip-wise image registration technique based on an earlier implementation (Stevenson et al., 2010). The images were combined into a roughly 1.5 x 1.5-degree foveal montage using both custom automontaging software (Chen et al., 2016) and manual blending in Corel Photo-Paint (CorelDRAW Graphics Suite 2019; Alludo, Ottawa, Canada) to reduce residual image distortions. In such montages, all cone center locations were annotated using ConeMapper, a custom neural network-assisted MATLAB tool for identifying cone locations (Gutnikov et al., 2025), followed by manual verification and correction. Cone density maps were generated via Voronoi diagrams, by averaging the area of the 150 closest cones to each pixel in the map. The cone density centroid (CDC), representing the anatomical foveal center, was determined as the weighted center of the top 20% cone density contour (Reiniger et al., 2021). The average distance to neighboring cones (inter-cone distance, ICD) was computed for every cone in the montage and employed for a trial-based estimation of each individual cone Nyquist limit (N_c) by, $N_c = ICD \times (\sqrt{3})/2$.

Stimuli and procedure

Visual acuity was assessed in a 4-alternative forced choice orientation discrimination of a tumbling-E optotype **(Fig. 1B)**. Throughout this manuscript, we define the stimulus size as the stroke width of the E. The stroke width corresponds to one-fifth of the full height of the optotype and is equal to the gap width between the limbs of the E. Orientation was varied pseudo-randomly and chosen from one of the four cardinal orientations (up, down, left, right) for each trial. Stimuli were

computationally constructed as bitmaps with a bit-depth close to 10 bits (1000 gray values). To achieve subpixel stimulus resolution, a Gaussian filter with a kernel size of five pixels and a sigma of one pixel was applied to the nominal stimulus (Guizar, 2025) before it was computationally resized to the desired value. To avoid border artefacts, stimuli were sufficiently zero-padded. A single stimulus presentation was initiated by the participant by a keyboard button press. After presentation, perceived orientation was reported using one of the four arrow keys on the keyboard (**Fig. 1A**).

Stimulus onset was during the eighth frame after trial initiation (i.e., after ~300ms) and were presented for 1, 3, 7, 11 or 16 AOSLO frames, which corresponds to a duration of approximately 3, 80, 220, 370, and 600 ms **(Fig. 2B, C).** In our AOSLO system, one video frame is composed of 512 lines, each sampled with 512 pixels, and is captured approximately every 37 milliseconds (frame rate: 27Hz). Stimuli are produced by turning the light source briefly off by acousto-optic modulation at appropriate times, corresponding to the pixel space. Most stimulus sizes were very small; the largest stimulus had a stroke width of 8 pixels (equaling 48 seconds of arc of visual angle, arcsec) and thus occupied less than 13% of the horizontal and vertical dimension of the raster. It took approximately 3 milliseconds for the laser to sweep across an area defined by such stimulus geometry (from top left to bottom right pixel). Despite the frame rate, stimuli spanning multiple frames were perceived by the observers as continuous and not flickering. Stimulus duration was thus defined as the time from when it first appeared to when it was switched off in the last frame. All stimuli were drawn at the center of the raster.

For each duration condition, an acuity threshold was determined in at least five repeated runs, with 23 trials per run. Stimulus size in each trial followed an adaptive staircase. Initial stimulus size was set to 48 arcsec. After each correct response, stimulus size was reduced by a factor of 1.75 until the first incorrect response, indicating the approximate region of the presumed threshold. From there, a two-down, one-up rule with 1.5 step size up and 0.82 step size down was applied (García-Pérez, 1998). Every sixth trial was a motivational stimulus where the stimulus was set to 48 arcsec (Bach, 1996). Before the experimental session,

participants did five test runs each consisting of 23 trials with a 500 ms presentation duration to become acquainted with the testing procedure.

Each dataset underwent curation prior to psychophysical analysis during which on average 30% of all recorded trials were removed from the analysis. Trials were excluded if saccades, microsaccades, or blinks occurred during stimulus presentation. Additionally, trials were removed if technical issues disrupted stimulus presentation, such as missing stimulus features or altered stimulus appearance on the retina, both possible artefacts of the stimulus delivery hardware. Trial elimination was performed using custom-written software that identified the time periods during which stimuli were presented, calculated eye movement velocity within those intervals and flagged trials where it exceeded 30 arcmin/s (indicating a micro saccade). Cross-correlation was used to compare the intended stimulus geometry with the stimulus as presented on the retina, allowing detection of distorted or missing presentations. Results of this procedure were verified by a human observer by inspecting each case visually. Trials across repeated runs were pooled and binned to yield at least seven representative bins. Bin sizes varied depending on the available stimulus sizes, with widths ranging from 5 to 11 arcsec, and were used to compute psychometric function fits. The visual acuity threshold, defined as the stimulus size required for 62.5% correct responses, was estimated by fitting the pooled data to a Weibull distribution function using the Matlab toolbox Psignifit (Wichmann & Hill, 2001). In general, lower threshold values indicate better acuity.

Ocular drift analysis

Eye motion traces were extracted from the one-second AOLSO videos by strip-wise image registration with a temporal resolution of 864 Hz (Stevenson & Roorda, 2005). Because of registration artefacts that are due to reference-frame distortions and ocular torsion (Hofmann et al., 2022), high-resolution motion traces were down-sampled by linear interpolation between the central samples in each frame. Retinal slip during stimulus presentation was quantified by the total slip exhibited, calculated as the sum of the concatenated drift motion vector lengths. To quantify drift variance, we first computed the mean squared displacement (MSD) for each trial. Then, at each time point, the variance across all MSD curves

from repeated presentations was calculated. This yielded a time-dependent measure of how drift dispersion evolved across trials. The drift-variance value reported corresponds to the variance at the 600-ms time point.

To better understand the role of cone photoreceptors directly involved when a stimulus is presented to the retina, we introduce a metric termed *seeing cones* **(Fig. 2A)**. Unique *seeing cones* per trial were found by examining all AOSLO video frames where the stimulus appeared. Subsequently, we registered these frames to an annotated cone montage to determine which cones were covered by the stimulus. We then applied a simple model of light capture, assigning each cone a light acceptance aperture, with its diameter estimated as 48% of the average spacing between neighboring cones, using a Gaussian approximation (Macleod et al., 1992). The retinal image was computed by convolving the eye's diffraction-limited point spread function (calculated for 788nm light and a 7 mm pupil) with the nominal stimulus. The retinal image was overlaid onto the cone aperture model and both matrices multiplied. The total light capture was calculated for each trial throughout all the frames when the stimulus was presented, and the percentage of light captured by each cone was determined. Cones that capture more than 1% of the total light – corresponding to the smallest detectable contrast (Fechner,1860; Pelli & Bex, 2013) – were classified as *seeing cones*.

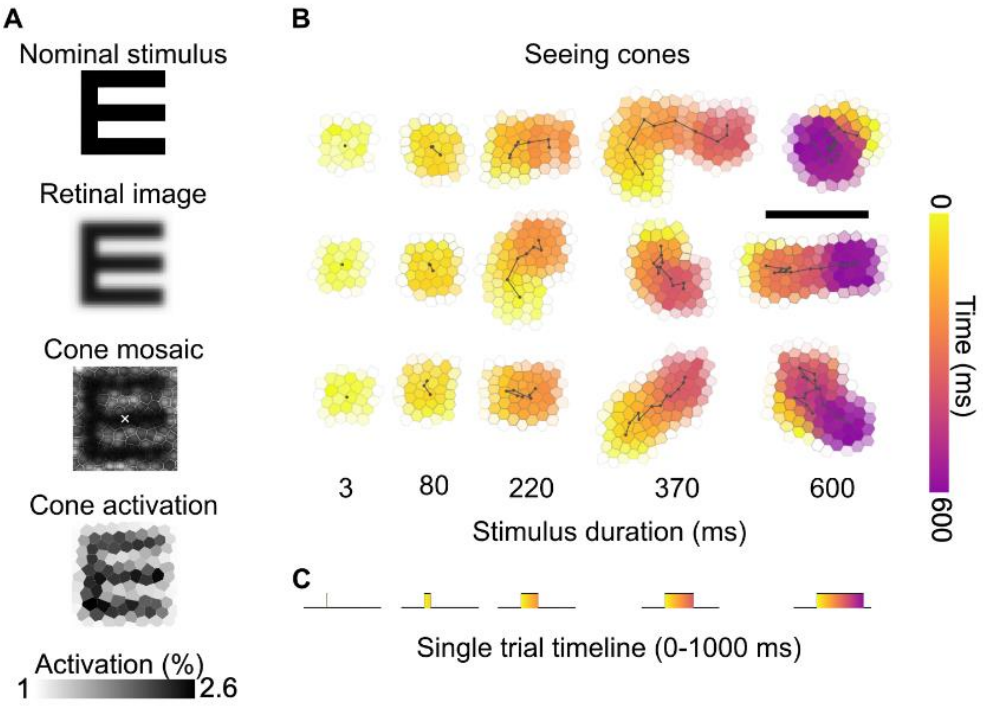

Figure 2. Cone activation and *seeing cones* across stimulus durations.
(A) Computation of single cone activation: the nominal stimulus is blurred by the eye's optics. Multiplication of the retinal stimulus with the underlying cone mosaic light apertures results in a cone-activation map. Because the E was presented in OFF contrast (a dark E on a red background), cones receiving less light show higher activation and therefore appear darker. The grayscale represents normalized activation (% of maximum cone activation). (B) *Seeing cones* were determined by cone-activation patterns over the course of exhibited drift trajectories. Three example trials (Participant P2) are shown at each stimulus duration. Each hexagonal cell represents a cone; the color indicates the time course of stimulus motion across the cone mosaic (yellow = early, purple = late). Black lines show the fixational drift trajectory during stimulus presentation. As duration increases, retinal slip covers progressively larger portions of the cone mosaic. Scale bar is 5 arcmin. (C) Single trial timeline, where a 1-second video is recorded. The stimulus onset occurs at approximately 300 ms and is presented for a variable duration, ranging from 3 to 600 ms.

In our simplified model we exclude considerations of a cone's temporal decay function. In AOSLO-based stimulus delivery, the stimulus is projected onto the retina by modulating the scanning laser's intensity, specifically by switching it off to deliver light decrements relative to the scanning raster as the laser traverses the retina (Poonja et al., 2005). Consequently, each retinal location within the scanning raster, excluding the stimulus delivery area, receives a single brief pulse of focused light within each frame cycle (approximately every 37 ms in our system if no movement occurred). We interpret the light decrements defining the stimulus as activation signals, based on the presence of equally distributed ON and OFF visual pathways in the foveola (Polyak, 1957). Even though a functional

asymmetry in activation between those pathways has been shown, we assumed that acuity performance is likely unaffected by such asymmetries (Chichilnisky & Kalmar, 2002; Patterson et al., 2025).

In the condition where stimuli were presented for a single frame (3 ms duration), we assumed the slip to be zero for the seeing cone calculation. This assumption likely holds: based on the observed average drift velocity of about 13 arcmin/s, a 3 ms duration would equate to less than 2.4 arcsec of exhibited slip, a displacement of less than a tenth of a single cone diameter on the retina.

Results

All participants exhibited significant differences in foveal anatomy, eye movement patterns, and visual acuity, highlighting individual variability in foveal structure and function (**Fig. 3, Table 1**).

Participant #	Cone density and Nyquist limit at CDC (cones/deg²)/(arcsec)	Drift velocity (arcmin/s)/(cones/s)	Drift length 600 ms (arcmin)	Drift variance (arcmin²)	Seeing cones (deg²)/(N)	ISOA to CDC distance (arcmin)
P1	11,749 / 30.9	17.5 / 31.2	10.2	1925	0.18 / 1793	7.2
P2	13,883 / 28.4	11.9 / 23.9	6.9	321	0.11 / 1422	1.2
P3	15,005 / 27.4	12.5 / 27.6	7.6	129	0.08 / 1140	0.94
P4	15,466 / 26.9	16.1 / 36.2	10	98	0.13 / 1677	4
P5	16,016 / 26.5	10 / 22.1	5.9	26	0.07 / 1043	2
P6	17,000 / 25.7	10.4 / 23.9	6.3	40	0.1 / 1476	0.86
P7	17,971 / 25	14 / 31.1	8.2	280	0.19 / 2690	4.8

Table 1. Cone mosaic and drift characteristics
For each participant, the table lists the cone density and corresponding Nyquist sampling limit at the center of the fovea (CDC), mean drift velocity, drift length at 600 ms, drift variance at 600 ms (dispersion of drift trajectories), angular subtense and total number of *seeing cones* engaged during the task, and the offset between the CDC and the centroid of the stimulus landing region (ISOA). Participant ocular drift and cone mosaic metrics.

Foveolar topography and retinal location

Foveal cone density, and hence sampling limits, differed markedly across participants, spanning from relatively sparse (11.8k, 31 arcsec) to dense (18k cones/deg^2, 25 arcsec) mosaics (**Fig. 3A**, **Table 1**). When a constant-size Snellen E was projected onto each retina, these differences highlighted how individual sampling limits might come into play. Because eye-movement patterns also varied, the retinal area used during the acuity task differed across observers (**Fig. 3B**). As a result, both the extent of the seeing region and the number of cones contributing to it varied (**Table 1**). Despite this, mostly a core subset of cones saw stimuli: those stimulated more than ten times accounted for 67-78% of all engaged cones.

Stimuli were also seen by different parts of the participants' retinas. The average location of all stimulus presentations across all trials, defined as the centroid of the isocontour area (ISOA) of 68% of stimulus landing points, varied in distance from the CDC (**Fig. 3B**, **Table 1**). The ISOA centroids for participants P1, P7, and P4 were located the farthest from the CDC, at distances of 7.2, 4.8, and 4 arcmin, respectively. In contrast, participants P2 and P5 positioned stimuli closer to the CDC, with shifts of 1.2 and 2.0 arcmin. Notably, participants P3 and P6 had ISOA centroids positioned less than 1 arcmin from the CDC.

Linear regression did not show a significant relationship between cone density at CDC and the total area covered by all *seeing cones* ($p = 0.8$) nor number of *seeing cones* ($p = 0.51$). Also, both area ($p = 0.053$) and number of *seeing cones* ($p = 0.25$) did not relate significantly to drift velocity. However, a significant relationship was observed between drift velocity and the distance from the ISOA centroid to the CDC: drift velocity was higher when the distance was larger ($R^2 = 0.74$, $p = 0.01$). Illustrations of all retinal slip trajectories for each duration condition demonstrate the individual use of retinal space over time, reflecting individual FEMs and their continuous presence throughout the visual task (**Fig. 3C**).

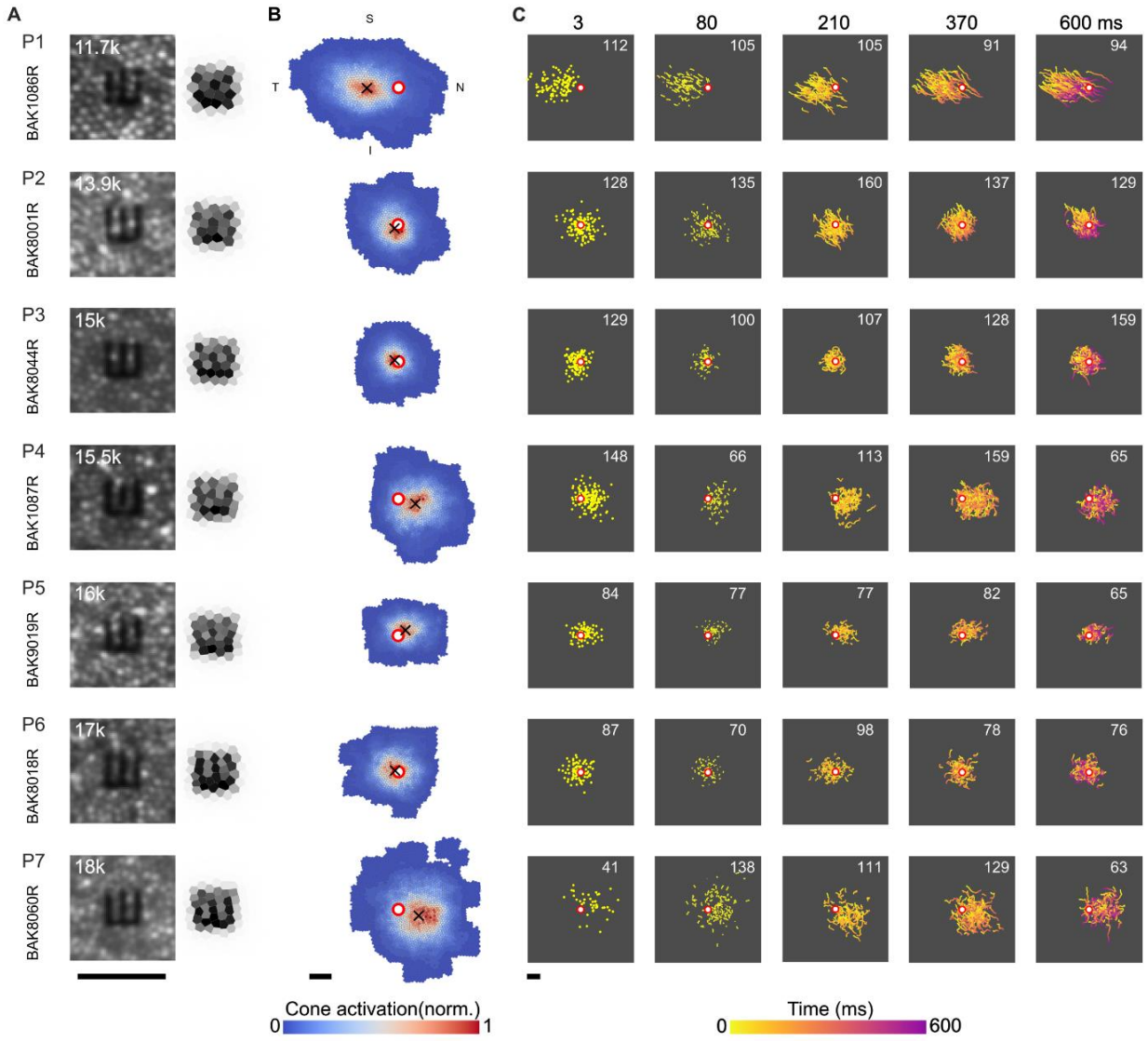

Figure 3. Retinal sampling and motion traces.
(A) AOSLO image crops for all participants (P1–P7, rows) centered on the CDC, with a 25-arcsec tumbling-E stimulus superimposed. The panels on the right show the corresponding cone-activation maps. Each hexagonal element represents an individual cone, and the grayscale value indicates the relative activation of that cone during a single frame. Cone density in cones/deg^2 at the CDC is indicated in the upper-left corner of each AOSLO image. (B) *Seeing cones* heatmaps across all trials. The CDC is indicated by the red-white circle marker. The ISOA centroid, i.e. the average stimulus location, is labeled with the black cross marker. Only right eyes were tested. (C) Motion traces for all trials across all participants. Columns are stimulus durations. The number shown within each panel denotes the count of valid trials. Color indicates time after stimulus onset. All scale bars are 5 arcmin.

Retinal slip and *seeing cones*

Individuals also showed substantial differences in their drift velocity, the amount of retinal distance traversed, and the temporal variability of their drift

trajectories. When averaged across all trials and conditions, retinal slip velocity ranged from 10 to 17.5 arcmin/s across participants, or equivalently, 22 to 36 cone diameters per second in the individual eye (**Table 1**). Velocities differed significantly between observers (Kruskal–Wallis Test, $\chi^2(6) = 1101.14$, $p < 0.001$) but did not vary systematically with stimulus duration within observers (all $p > 0.05$). On average, drift length rose steadily across the four longer durations, but participants differed substantially in the magnitude of this increase. Variability was most pronounced at 600 ms, where drift lengths spanned a wide range (**Fig.4A, Table 1**). At this duration, drift length correlated positively with the distance between each observer's ISOA centroid and CDC ($R^2 = 0.67$, $p = 0.025$). At 600 ms, the log-transformed drift variance showed an inverse relationship with cone density at the CDC ($R^2 = 0.6$, $p = 0.04$): participants with higher cone density exhibited smaller positional variance over time, whereas those with sparser mosaics displayed greater dispersion (**Fig. 4B, Table 1**).

To examine how drift affects the spatial extent of retinal sampling, we quantified the number of cones stimulated over time on a trial-by-trial basis (**Fig. 4C**). In principle, observers with higher cone density or faster drift would be expected to activate more cones than those with slower drift or sparser mosaics. To isolate inter-individual anatomical differences, we restricted this analysis to acuity targets between 24–36 arcsec. For the ultra-brief 3 ms duration, the number of *seeing cones* increased with higher cone density ($R^2 = 0.87$, $p = 0.002$), as expected (**Fig. 4D**). However, for the 80–600 ms durations, no significant relationship was found between cone density and the number of *seeing cones*. Taken together with the drift-variance analysis, these results indicate that the slip exhibited by each eye partially reduced the anatomical differences in cone density across participants, contributing to a more consistent number of *seeing cones* at

the longer durations.

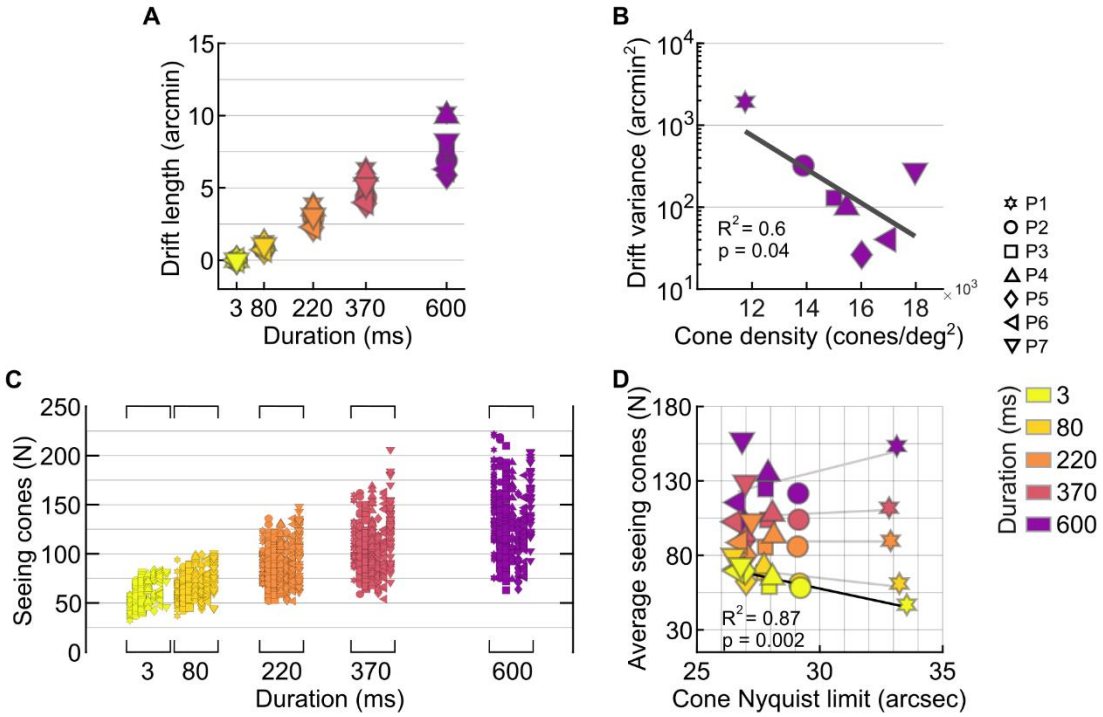

Figure 4. Drift characteristics and *seeing cones*.
(A) Average retinal slip length for each participant (marker type) is plotted against presentation duration (color). Retinal slip grew linearly and varied among individuals, peaking at 600 ms, where it reached an average of 7.8 ± 2 arcmin and the difference between those with the lowest and highest retinal slip reached a factor of 1.7. (B) Drift variance at 600ms as the function of cone density at the CDC. The black line shows the linear regression fit. (C) *Seeing cones* plotted for individual trials where stimulus size ranged between 24-36 arcsec for each participant. Each data column is one participant. (D) Average *seeing cones* as a function of individual cone density given as their Nyquist limit. Black line indicates linear regression model fits where $p < 0.05$, gray lines indicate non-significant correlations.

Acuity thresholds at different stimulus durations

Acuity improved with increasing presentation duration in all participants, but performance changed abruptly between the ultra-brief 3 ms condition and 80 ms (**Fig. 5A**). At 3 ms, thresholds clustered close to each observer's cone-sampling limit, and normalization to the individual Nyquist limit reduced inter-participant variability (**Fig. 5B**), indicating that cone topography constrained performance when essentially no retinal slip occurred. At 80 ms, thresholds for most participants fell below their cone Nyquist limits, and they continued to improve with longer durations. Beyond this transition, cone density no longer predicted

threshold differences. For the three longest durations, thresholds settled into a narrow range across observers, corresponding to roughly 0.8-0.75 of the Nyquist limit. The selective reduction in variability at 3 ms **(Fig. 5 A,B)** and the significant correlation at this duration ($R^2 = 0.66$, $p = 0.026$; **Fig. 5C**) reinforce that cone sampling was limiting only at zero drift.

Across participants, thresholds improved when areas of higher cone densities were used (**Fig.5D**). When the ratio between the average ICD across trials in a given condition and the ICD at the CDC was calculated, we found a significant relationship between threshold and such ratio for the 3 ($R^2 = 0.57$, $p = 0.05$), 220 ($R^2 = 0.9$, $p = 0.0004$), 370 ($R^2 = 0.7$, $p = 0.02$), and 600 ($R^2 = 0.77$, $p = 0.009$) ms durations. For the 80 ms presentation duration, the relationship was not significant ($p = 0.13$), although the trend was similar.

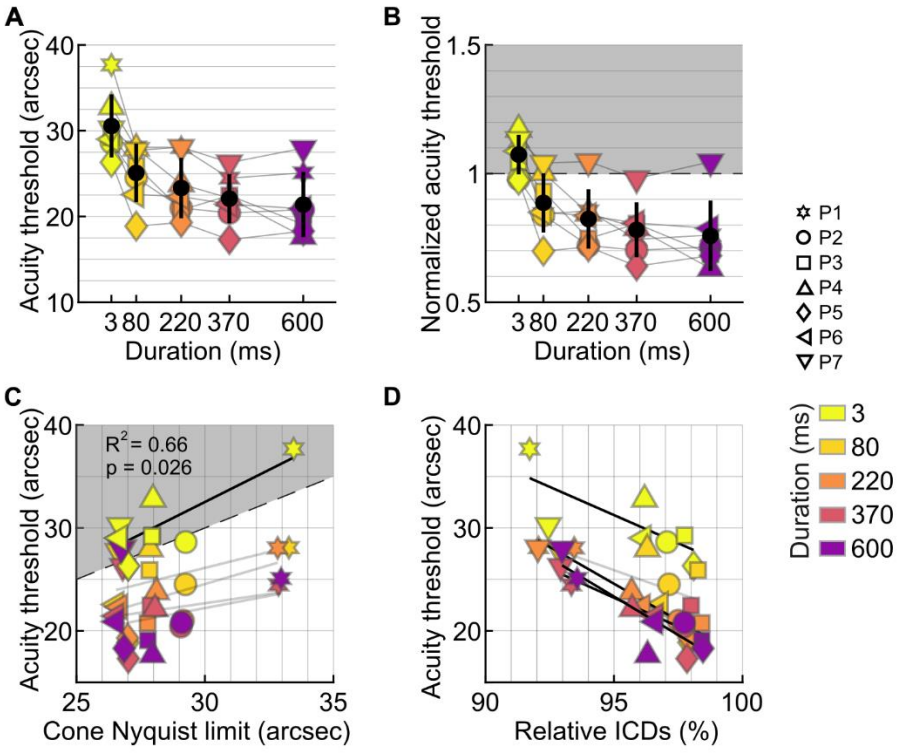

Figure 5. Acuity at different stimulus durations.
(A) Absolute acuity thresholds as function of presentation duration in all participants. Black markers are average and standard deviation across participants per condition. (B) Acuity threshold normalized to the individual cone Nyquist limit. The gray area indicates acuity values above the Nyquist limit (normalized values > 1), corresponding to performance worse than the cone-resolution limit. (C) Acuity as a function of the cone sampling limit. Linear regression was only significant for the flash

condition (3 ms). (D) Acuity as a function of the ratio between inter-cone distances (ICDs) of *seeing cones* and ICDs at the CDC.

Discussion

Using adaptive optics micro-psychophysics combined with simultaneous in vivo imaging of the moving human retina, we measured tumbling-E acuity at varying stimulus durations. We found that sub-Nyquist acuity can be reached at durations as short as 80 ms, corresponding to a retinal slip of less than 1 arcmin, about two foveal cone diameters.

Cone mosaic limits performance in the absence of FEM

The Nyquist limit represents a theoretical upper bound of visual resolution and has long been considered a fundamental constraint on visual acuity (Westheimer, 1975; Strasburger et al., 2018). By varying stimulus presentation duration, we found that acuity thresholds closely matched the individual Nyquist limit (**Fig. 5B**) only when the stimulus remained effectively stationary on the retina (3 ms). In the absence of retinal slip, the density of the retinal sampling array must exceed that of the stimulus to allow un-aliased signal reconstruction. Otherwise, undersampling may introduce perceptual distortions (but see Ruderman & Bialek, 1992) that mask the true form.

We found that individual retinal sampling limits were surpassed once stimuli were allowed to move on the retina, except in one participant (P7, who seemed an outlier, see below) (**Fig. 5B**). These results confirmed previous findings obtained under optimal optical conditions using AOSLO (Rossi et al., 2007; Witten et al., 2024). Earlier observations with optics independent interference stimulation showed that line patterns remained detectable up to 90–100 cycles/deg, corresponding to a spacing of 18–20 arcsec (Williams, 1985). Such thresholds and our observed sub-Nyquist acuities are likely achievable through a dynamic de-alias, where fixational eye movements engage multiple photoreceptors over time and effectively remove artifacts that are due to undersampling.

Minimal retinal slip has highest impact on threshold

We found that when stimuli slip on the retina, thresholds decreased, i.e., acuity improved. The most pronounced improvement was observed between the 3 ms and 80 ms presentation durations, with a threshold decrease by 17.5%, on average. At 80 ms, stimulus slip was less than 1 arcmin, on average, less than two foveal cone diameters (**Fig. 4A**). This finding suggests that even minimal retinal slip can enhance spatial sampling by shifting the stimulus across adjacent cones within a short time window. This is in line with earlier behavioral reports (Kuang et al., 2012; Intoy & Rucci, 2020) and theoretical modeling (Pitkow et al., 2007; Ahissar & Arieli, 2012; Nghiem et al., 2025), demonstrating that a retinal slip imposed by FEM aids acuity. The necessary slip amplitudes have been shown to be minimal, and do not necessarily have to be stemming from an individual's own eye motion to aid acuity (Ratnam et al., 2017).

When stimulus slip amplitudes are modulated by varying the duration the stimulus is visible, temporal information integration must be taken into account. According to Bloch's law, longer exposures, even at the same intensity, improve detectability of small stimuli (Gorea, 2015). A prominent mechanism thought to be at play here is probability summation, where multiple weak or sub-threshold signals are combined to increase signal strength (Watson, 1979). Temporal integration was shown to improve performance only with short presentation durations, up to a critical duration reported between 50 to 100 ms (Barlow, 1958; Saunders, 1975; Gorea, 2015), after which partial summation persists up to 650 ms (Holmes et al., 2017). Similar results emerged in our study, where threshold improvement rates declined beyond ~80 ms.

In our experiments, performance continued to improve as the duration of stimulus presentation increased (**Fig. 5 A,B**). However, the relative gains between successive durations decreased and were not statistically significant, with improvements of 7%, 5.4%, and 3% for the longer durations, compared to an improvement of 17.5% from 3 ms to 80 ms. Prior studies reinforce the notion of a nonlinear temporal integration process, where most perceptual benefits are achieved within the first ~100 ms of stimulus visibility (Tulunay-Keesey & Jones, 1976; Ng & Westheimer, 2002), after which acuity increases with a gradually decreasing rate (Baron & Westheimer, 1973; Alexander et al., 1993; Niwa & Tokoro, 1997; Heinrich

et al., 2010; McAnany, 2014). Our findings align with the principle of nonlinear temporal integration with continued temporal summation (Holmes et al., 2017) in the visual system.

Interactions between cone topography and FEM

We observed that the benefit of a denser cone mosaic was no longer visible at longer stimulus durations (**Fig. 5C**). At these timescales, neither cone topography nor movement statistics alone predicted acuity. Instead, a more complex picture emerged in which cone topography, retinal location, and movement patterns interacted.

One key aspect of this interaction was the relationship between drift direction and cone topography: stimuli that were displaced toward regions of higher cone density were associated with better acuity (**Fig. 5D**). This implies that participants often relied on retinal regions with lower cone density than their theoretical maximum, providing on average ~95% of their available cone sampling capacity. Indeed, the centroid of *seeing cones* was consistently offset from the anatomical center by 1–7.2 arcmin across participants. Those with the largest offsets (7.2 and 4.8 arcmin in P1 and P7) also exhibited the highest thresholds. Such offset fixation appears to be a typical feature of human vision, occurring symmetrically across eyes, but it remains unclear if it serves a particular role (Putnam et al., 2005; Wilk et al., 2017; Wang et al., 2019; Kilpeläinen et al., 2020; Reiniger et al., 2021).

The displacement of the stimulation centroid was further linked to drift velocity ($R^2 = 0.74$, $p = 0.01$) and drift length at long durations ($R^2 = 0.67$, $p = 0.025$). These findings indicate that relatively large fixational eye movements can reduce acuity, consistent with previous reports (Clark et al., 2022). Higher FEM velocities tended to shift gaze toward more peripheral retinal regions, where cone size increases and spatial resolution decreases (Rossi & Roorda, 2010; Intoy & Rucci, 2020), even when the displacements occurred within the foveola (Jenks et al., 2025). As a consequence, performance differences could also reflect a reduced ganglion cell–to–cone ratio in the foveola. Although a uniform 2:1 ratio is often assumed (Curcio & Allen, 1990; McCann et al., 2011; Watson, 2014), recent work suggests higher values and greater variability (Drasdo et al., 2007). Together with emerging evidence

of idiosyncratic foveolar cone topography and their functional employment (Ameln et al., 2025; Witten et al. 2024; Reiniger et al., 2021) and asymmetries in visual performance (Jenks et al., 2025), these results point to the need for finer distinctions within foveolar circuitry.

Individual participants further illustrate how FEMs can either aid or harm performance. P7, for example, exhibited fast movements over high-density regions and rarely reached sub-Nyquist acuity (**Fig. 5B**)**.** Having also the highest number of uniquely activated cones, this combination may exceed optimal cone signals (Pitkow et al., 2007; Burak et al., 2010). In contrast, participant P1 with lower baseline cone sampling but equally high drift velocity and highest drift variance was able to reach sub-Nyquist thresholds, although their stimulus centroid remained displaced from the densest regions. Interestingly, at 600 ms, both P1 and P7 recruited similar numbers of cones for stimulus sizes between 24–36 arcsec, despite P7 having 35% higher cone density at the CDC (**Fig. 4C**). Thus, FEMs acted as an equalizing factor: for P1 they may have enhanced performance by engaging more cones, while for P7 they may have limited the benefit of higher local density. Finally, participants showed consistent and habitual use of retinal areas which display consistent ICDs, evidenced by the low variability in *seeing cone* densities across conditions (**Fig. 4C**). Similarly, a stable proportion of cones (67–78%) was recruited throughout trials (**Fig. 3B**). Together with the stereotypical drift patterns observed in P1, P2, and P3 (**Fig. 3C**), these findings suggest that individuals develop characteristic, habitual drift strategies, which may supersede optimal, trial by trial trajectories.

Conclusions

In this study, we investigated how stimulus duration, fixational eye movements, and local cone topography jointly impact foveal visual acuity. We found that visual acuity benefits from naturally occurring fixational eye movements within the first 80 ms of viewing, during which the stimulus is displaced by less than 1 arcmin, corresponding to only about two diameters of the smallest foveal cones. Remarkably, this minimal retinal slip was already sufficient to improve performance from the static, cone-limited regime to sub-Nyquist acuity levels. Beyond this initial

interval, acuity continued to improve with increasing stimulus duration, albeit at a reduced rate.

Fixational drift characteristics varied substantially across participants, and their impact on acuity depended on how individual drift trajectories interacted with local cone topography and retinal location. At longer stimulus durations, neither cone density nor drift magnitude alone predicted performance; rather, acuity reflected the combined effect of where stimuli landed, how they moved relative to regions of higher or lower cone density, and the individual's habitual drift strategy. Consistent with this interplay, observers with denser mosaics often drifted across smaller retinal regions, which led to a reduction in the spread of engaged cones across participants.

Together, our findings show that fixational eye movements can both aid and limit visual acuity depending on the timescale. Most importantly, they demonstrate that the visual system can extract meaningful spatial information from extremely small retinal displacements, highlighting the critical role of even minimal drift in shaping foveal vision over brief viewing intervals.

References

Ahissar, E., & Arieli, A. (2001). Figuring space by time. Neuron, 32(2), 185–201. https://doi.org/10.1016/s0896-6273(01)00466-4

Ahissar, E., & Arieli, A. (2012). Seeing via Miniature Eye Movements: A Dynamic Hypothesis for Vision. Frontiers in Computational Neuroscience, 6, 89. https://doi.org/10.3389/fncom.2012.00089

Alexander, K. R., Derlacki, D. J., Fishman, G. A., & Szlyk, J. P. (1993). Temporal properties of letter identification in retinitis pigmentosa. Journal of the Optical Society of America A, 10(7), 1631–1636. https://doi.org/10.1364/JOSAA.10.001631

Ameln, J., Witten, J. L., Gutnikov, A., Lukyanova, V., Holz, F. G., & Harmening, W. M. (2025). In Vivo Cone Photoreceptor Topography of the Human

608 Foveola. Investigative Ophthalmology & Visual Science, 66(11), 13.
609 https://doi.org/10.1167/iovs.66.11.13
610 Anderson, A. G., Ratnam, K., Roorda, A., & Olshausen, B. A. (2020). High-acuity
611 vision from retinal image motion. Journal of Vision, 20(7), 34.
612 https://doi.org/10.1167/jov.20.7.34
613 Arathorn, D. W., Yang, Q., Vogel, C. R., Zhang, Y., Tiruveedhula, P., & Roorda,
614 A. (2007). Retinally stabilized cone-targeted stimulus delivery. Optics
615 Express, 15(21), 13731–13744. https://doi.org/10.1364/oe.15.013731
616 Bach, M. (1996). The Freiburg Visual Acuity test: Automatic measurement of
617 visual acuity. Optometry and Vision Science, 73(1), 49–53.
618 https://doi.org/10.1097/00006324-199601000-00008
619 Barlow, H. B. (1958). Temporal and spatial summation in human vision at
620 different background intensities. The Journal of Physiology, 141(2), 337–350.
621 https://doi.org/10.1113/jphysiol.1958.sp005978
622 Baron, W. S., & Westheimer, G. (1973). Visual acuity as a function of exposure
623 duration. Journal of the Optical Society of America, 63(2), 212–219.
624 https://doi.org/10.1364/JOSA.63.000212
625 Ben-Shushan, N., Shaham, N., Joshua, M., & Burak, Y. (2022). Fixational drift is
626 driven by diffusive dynamics in central neural circuitry. Nature
627 Communications, 13(1), 1697. https://doi.org/10.1038/s41467-022-29201-y
628 Burak, Y., Rokni, U., Meister, M., & Sompolinsky, H. (2010). Bayesian model of
629 dynamic image stabilization in the visual system. Proceedings of the National
630 Academy of Sciences of the United States of America, 107(45), 19525–
631 19530. https://doi.org/10.1073/pnas.1006076107

Campbell, F. W., & Green, D. G. (1965). Optical and retinal factors affecting visual resolution. The Journal of Physiology, 181(3), 576–593. https://doi.org/10.1113/jphysiol.1965.sp007784

Chen, M., Cooper, R. F., Han, G. K., Gee, J., Brainard, D. H., & Morgan, J. I. W. (2016). Multi-modal automatic montaging of adaptive optics retinal images. Biomedical Optics Express, 7(12), 4899–4918. https://doi.org/10.1364/BOE.7.004899

Chichilnisky, E. J., & Kalmar, R. S. (2002). Functional asymmetries in ON and OFF ganglion cells of primate retina. The Journal of Neuroscience, 22(7), 2737–2747. https://doi.org/10.1523/JNEUROSCI.22-07-02737.2002

Clark, A. M., Intoy, J., Rucci, M., & Poletti, M. (2022). Eye drift during fixation predicts visual acuity. Proceedings of the National Academy of Sciences of the United States of America, 119(49), e2200256119. https://doi.org/10.1073/pnas.2200256119

Curcio, C. A., & Allen, K. A. (1990). Topography of ganglion cells in human retina. Journal of Comparative Neurology, 300(1), 5–25. https://doi.org/10.1002/cne.903000103

Ditchburn, R. W., & Ginsborg, B. L. (1952). Vision with a Stabilized Retinal Image. Nature, 170(4314), 36–37. https://doi.org/10.1038/170036a0

Dodge, R. (1907). An experimental study of visual fixation. The Psychological Review: Monograph Supplements, 8(4), i–95. https://doi.org/10.1037/h0093042

Domdei, N., Reiniger, J. L., Holz, F. G., & Harmening, W. M. (2021). The Relationship Between Visual Sensitivity and Eccentricity, Cone Density and

656 Outer Segment Length in the Human Foveola. Investigative Ophthalmology &
657 Visual Science, 62(9), 31. https://doi.org/10.1167/iovs.62.9.31
658 Drasdo, N., Millican, C. L., Katholi, C. R., & Curcio, C. A. (2007). The length of
659 Henle fibers in the human retina and a model of ganglion receptive field
660 density in the visual field. Vision Research, 47(22), 2901–2911.
661 https://doi.org/10.1016/j.visres.2007.01.007
662 Engbert, R., Mergenthaler, K., Sinn, P., & Pikovsky, A. (2011). An integrated
663 model of fixational eye movements and microsaccades. Proceedings of the
664 National Academy of Sciences of the United States of America, 108(39),
665 E765–770. https://doi.org/10.1073/pnas.1102730108
666 Fechner, G. T. (1966). Elements of psychophysics (H. E., Adler,D. H., Howes,E.
667 G. Boring,). New York, NY: Holt, Rinehart & Winston. (Original work published
668 1860)
669 García-Pérez, M. A. (1998). Forced-choice staircases with fixed step sizes:
670 Asymptotic and small-sample properties. Vision Research, 38(12), 1861–
671 1881. https://doi.org/10.1016/s0042-6989(97)00340-4
672 Gorea, A. (2015). A Refresher of the Original Bloch's Law Paper (Bloch, July
673 1885). I-Perception, 6(4), 2041669515593043.
674 https://doi.org/10.1177/2041669515593043
675 Gutnikov, A., Hähn-Schumacher, P., Ameln, J., Zadeh, S. G., Schultz, T., &
676 Harmening, W. (2025). Neural network assisted annotation and analysis tool
677 to study in-vivo foveolar cone photoreceptor topography. Scientific Reports,
678 15(1), 23858. https://doi.org/10.1038/s41598-025-08028-9

679 Hafed, Z. M., Chen, C.-Y., Tian, X., Baumann, M. P., & Zhang, T. (2021). Active
680 vision at the foveal scale in the primate superior colliculus. Journal of
681 Neurophysiology, 125(4), 1121–1138. https://doi.org/10.1152/jn.00724.2020
682 Hammer, D. X., Ferguson, R. D., Bigelow, C. E., Iftimia, N. V., Ustun, T. E., &
683 Burns, S. A. (2006). Adaptive optics scanning laser ophthalmoscope for
684 stabilized retinal imaging. Optics Express, 14(8), 3354–3367.
685 https://doi.org/10.1364/OE.14.003354
686 Heckenmueller, E. G. (1965). Stabilization of the retinal image: A review of
687 method, effects, and theory. Psychological Bulletin, 63(3), 157–169.
688 https://doi.org/10.1037/h0021743
689 Heinrich, S. P., Krüger, K., & Bach, M. (2010). The effect of optotype
690 presentation duration on acuity estimates revisited. Graefe's Archive for
691 Clinical and Experimental Ophthalmology, 248(3), 389–394.
692 https://doi.org/10.1007/s00417-009-1268-2
693 Hofmann, J., Domdei, L., Jainta, S., & Harmening, W. M. (2022). Assessment of
694 binocular fixational eye movements including cyclotorsion with split-field
695 binocular scanning laser ophthalmoscopy. Journal of Vision, 22(10), 5.
696 https://doi.org/10.1167/jov.22.10.5
697 Holmes, R., Victora, M., Wang, R. F., & Kwiat, P. G. (2017). Measuring temporal
698 summation in visual detection with a single-photon source. Vision Research,
699 140, 33–43. https://doi.org/10.1016/j.visres.2017.06.011
700 Intoy, J., & Rucci, M. (2020). Finely tuned eye movements enhance visual
701 acuity. Nature Communications, 11(1), 795. https://doi.org/10.1038/s41467-
702 020-14616-2

Jenks, S. K., Carrasco, M., & Poletti, M. (2025). Asymmetries in foveal vision. Journal of Neuroscience. https://doi.org/10.1523/JNEUROSCI.0055-25.2025

Keesey, U. T. (1960). Effects of Involuntary Eye Movements on Visual Acuity. Journal of the Optical Society of America, 50(8), 769–774. https://doi.org/10.1364/JOSA.50.000769

Kelly, D. H. (1979). Motion and vision. I. Stabilized images of stationary gratings. Journal of the Optical Society of America, 69(9), 1266–1274. https://doi.org/10.1364/JOSA.69.001266

Kilpeläinen, M., Putnam, N. M., Ratnam, K., & Roorda, A. (2020). The Anatomical, Functional and Perceived Location of the Fovea in the Human Visual System (SSRN Scholarly Paper No. 3699785). Social Science Research Network. https://doi.org/10.2139/ssrn.3699785

Kuang, X., Poletti, M., Victor, J. D., & Rucci, M. (2012). Temporal encoding of spatial information during active visual fixation. Current Biology: CB, 22(6), 510–514. https://doi.org/10.1016/j.cub.2012.01.050

Macleod, D. I. A., Williams, D. R., & Makous, W. (1992). A visual nonlinearity fed by single cones. Vision Research, 32(2), 347–363. https://doi.org/10.1016/0042-6989(92)90144-8

Malevich, T., Buonocore, A., & Hafed, Z. M. (2020). Rapid stimulus-driven modulation of slow ocular position drifts. eLife, 9, e57595. https://doi.org/10.7554/eLife.57595

Guizar, M. (2025). *Efficient subpixel image registration by cross-correlation* [Computer software]. MATLAB Central File Exchange. https://www.mathworks.com/matlabcentral/fileexchange/18401-efficient-subpixel-image-registration-by-cross-correlation

728 Martinez-Conde, S., Macknik, S. L., & Hubel, D. H. (2004). The role of fixational
729 eye movements in visual perception. Nature Reviews. Neuroscience, 5(3),
730 229–240. https://doi.org/10.1038/nrn1348
731 McAnany, J. J. (2014). The effect of exposure duration on visual acuity for letter
732 optotypes and gratings. Vision Research, 105, 86–91.
733 https://doi.org/10.1016/j.visres.2014.08.024
734 McCann, B. C., Hayhoe, M. M., & Geisler, W. S. (2011). Decoding natural
735 signals from the peripheral retina. Journal of Vision, 11(10), 19.
736 https://doi.org/10.1167/11.10.19
737 Murakami, I., & Cavanagh, P. (1998). A jitter after-effect reveals motion-based
738 stabilization of vision. Nature, 395(6704), 798–801.
739 https://doi.org/10.1038/27435
740 Murakami, I., & Cavanagh, P. (2001). Visual jitter: Evidence for visual-motion-
741 based compensation of retinal slip due to small eye movements. Vision
742 Research, 41(2), 173–186. https://doi.org/10.1016/s0042-6989(00)00237-6
743 Nachmias, J. (1961). Determiners of the drift of the eye during monocular
744 fixation. Journal of the Optical Society of America, 51, 761–766.
745 https://doi.org/10.1364/josa.51.000761
746 Ng, J., & Westheimer, G. (2002). Time course of masking in spatial resolution
747 tasks. Optometry and Vision Science: Official Publication of the American
748 Academy of Optometry, 79(2), 98–102. https://doi.org/10.1097/00006324-
749 200202000-00011
750 Nghiem, T.-A. E., Witten, J. L., Dufour, O., Harmening, W. M., & Azeredo da
751 Silveira, R. (2025). Fixational eye movements as active sensation for high

visual acuity. Proceedings of the National Academy of Sciences, 122(6), e2416266122. https://doi.org/10.1073/pnas.2416266122

Niwa, K., & Tokoro, T. (1997). Measurement of temporal summation of visual acuity with use of modified tachistoscope. Japanese Journal of Ophthalmology, 41(6), 403–408. https://doi.org/10.1016/s0021-5155(97)00082-8

Packer, O., & Williams, D. R. (1992). Blurring by fixational eye movements. Vision Research, 32(10), 1931–1939. https://doi.org/10.1016/0042-6989(92)90052-K

Patterson, S. S., Cai, Y., Yang, Q., Merigan, W. H., & Williams, D. R. (2025). Asymmetric activation of retinal ON and OFF pathways by AOSLO raster-scanned visual stimuli. Biomedical Optics Express, 16(7), 2663–2691. https://doi.org/10.1364/BOE.566008

Pelli, D. G., & Bex, P. (2013). Measuring contrast sensitivity. Vision Research, 90, 10–14. https://doi.org/10.1016/j.visres.2013.04.015

Pitkow, X., Sompolinsky, H., & Meister, M. (2007). A Neural Computation for Visual Acuity in the Presence of Eye Movements. PLOS Biology, 5(12), e331. https://doi.org/10.1371/journal.pbio.0050331

Polyak, S. L. (1957). The vertebrate visual system: Its origin, structure, and function and its manifestations in disease. University of Chicago Press.

Poonja, S., Patel, S., Henry, L., & Roorda, A. (2005). Dynamic visual stimulus presentation in an adaptive optics scanning laser ophthalmoscope. *Journal of Refractive Surgery, 21*(5), S575–S580. https://doi.org/10.3928/1081-597X-20050901-30

776 Pritchard, R. M. (1961, June 1). Pritchard, R. M. (1961, June). Stabilized images
777 on the retina. *Scientific American, 204*, 72–78.
778 https://www.scientificamerican.com/article/stabilized-images-on-the-retina/
779 Putnam, N. M., Hofer, H. J., Doble, N., Chen, L., Carroll, J., & Williams, D. R.
780 (2005). The locus of fixation and the foveal cone mosaic. Journal of Vision,
781 5(7), 3. https://doi.org/10.1167/5.7.3
782 Ratnam, K., Domdei, N., Harmening, W. M., & Roorda, A. (2017). Benefits of
783 retinal image motion at the limits of spatial vision. Journal of Vision, 17(1), 30.
784 https://doi.org/10.1167/17.1.30
785 Reiniger, J. L., Domdei, N., Holz, F. G., & Harmening, W. M. (2021). Human
786 gaze is systematically offset from the center of cone topography. Current
787 Biology: CB, 31(18), 4188-4193.e3. https://doi.org/10.1016/j.cub.2021.07.005
788 Riggs, L. A., Ratliff, F., Cornsweet, J. C., & Cornsweet, T. N. (1953). The
789 Disappearance of Steadily Fixated Visual Test Objects. Journal of the Optical
790 Society of America, 43(6), 495–501. https://doi.org/10.1364/JOSA.43.000495
791 Rolfs, M. (2009). Microsaccades: Small steps on a long way. Vision Research,
792 49(20), 2415–2441. https://doi.org/10.1016/j.visres.2009.08.010
793 Roorda, A., Romero-Borja, F., Iii, W. J. D., Queener, H., Hebert, T. J., &
794 Campbell, M. C. W. (2002). Adaptive optics scanning laser ophthalmoscopy.
795 Optics Express, 10(9), 405–412. https://doi.org/10.1364/OE.10.000405
796 Rossi, E. A., & Roorda, A. (2010). The relationship between visual resolution
797 and cone spacing in the human fovea. Nature Neuroscience, 13(2), 156–157.
798 https://doi.org/10.1038/nn.2465

Rossi, E. A., Weiser, P., Tarrant, J., & Roorda, A. (2007). Visual performance in emmetropia and low myopia after correction of high-order aberrations. Journal of Vision, 7(8), 14. https://doi.org/10.1167/7.8.14

Rucci, M., Iovin, R., Poletti, M., & Santini, F. (2007). Miniature eye movements enhance fine spatial detail. Nature, 447(7146), 852–855. https://doi.org/10.1038/nature05866

Rucci, M., & Poletti, M. (2015). Control and Functions of Fixational Eye Movements. Annual Review of Vision Science, 1(Volume 1, 2015), 499–518. https://doi.org/10.1146/annurev-vision-082114-035742

Rucci, M., & Victor, J. D. (2015). The unsteady eye: An information-processing stage, not a bug. Trends in Neurosciences, 38(4), 195–206. https://doi.org/10.1016/j.tins.2015.01.005

Ruderman, D. L., & Bialek, W. (1992). Seeing beyond the Nyquist limit. Neural Computation, 4(5), 682–690. https://doi.org/10.1162/neco.1992.4.5.682

Saunders, R. McD. (1975). The critical duration of temporal summation in the human central fovea. Vision Research, 15(6), 699–703. https://doi.org/10.1016/0042-6989(75)90287-4

Stevens, J. K., Emerson, R. C., Gerstein, G. L., Kallos, T., Neufeld, G. R., Nichols, C. W., & Rosenquist, A. C. (1976). Paralysis of the awake human: Visual perceptions. Vision Research, 16(1), 93–98. https://doi.org/10.1016/0042-6989(76)90082-1

Stevenson, S. B., & Roorda, A. (2005). Correcting for miniature eye movements in high-resolution scanning laser ophthalmoscopy. Ophthalmic Technologies XV (Vol. 5688, pp. 145–151) . https://doi.org/10.1117/12.591190

Stevenson, S. B., Roorda, A., & Kumar, G. (2010). Eye tracking with the adaptive optics scanning laser ophthalmoscope. Proceedings of the 2010 Symposium on Eye-Tracking Research & Applications, 195–198. https://doi.org/10.1145/1743666.1743714

Strasburger, H., Huber, J., & Rose, D. (2018). Ewald Hering's (1899) On the Limits of Visual Acuity: A Translation and Commentary: With a Supplement on Alfred Volkmann's (1863) Physiological Investigations in the Field of Optics. I-Perception, 9(3), 2041669518763675. https://doi.org/10.1177/2041669518763675

Tulunay-Keesey, U., & Jones, R. M. (1976). The effect of micromovements of the eye and exposure duration on contrast sensitivity. Vision Research, 16(5), 481–488. https://doi.org/10.1016/0042-6989(76)90026-2

Tuten, W. S., & Harmening, W. M. (2021). Foveal vision. Current Biology: CB, 31(11), R701–R703. https://doi.org/10.1016/j.cub.2021.03.097

Walls, G. L. (1942). *The vertebrate eye and its adaptive radiation*. Cranbrook Institute of Science. https://doi.org/10.5962/bhl.title.7369

Wang, Y., Bensaid, N., Tiruveedhula, P., Ma, J., Ravikumar, S., & Roorda, A. (2019). Human foveal cone photoreceptor topography and its dependence on eye length. eLife, 8, e47148. https://doi.org/10.7554/eLife.47148

Watson, A. B. (1979). Probability summation over time. Vision Research, 19(5), 515–522. https://doi.org/10.1016/0042-6989(79)90136-6

Watson, A. B. (2014). A formula for human retinal ganglion cell receptive field density as a function of visual field location. Journal of Vision, 14(7), 15. https://doi.org/10.1167/14.7.15

Westheimer, G. (1975). Editorial: Visual acuity and hyperacuity. Investigative Ophthalmology & Visual Science, 14(8), 570–572.

Westheimer, G. (2009). Visual acuity: Information theory, retinal image structure and resolution thresholds. Progress in Retinal and Eye Research, 28(3), 178–186. https://doi.org/10.1016/j.preteyeres.2009.04.001

Westheimer, G., & McKee, S. P. (1975). Visual acuity in the presence of retinal-image motion. Journal of the Optical Society of America, 65(7), 847–850. https://doi.org/10.1364/josa.65.000847

Wichmann, F. A., & Hill, N. J. (2001). The psychometric function: I. Fitting, sampling, and goodness of fit. Perception & Psychophysics, 63(8), 1293–1313. https://doi.org/10.3758/BF03194544

Wilk, M. A., Dubis, A. M., Cooper, R. F., Summerfelt, P., Dubra, A., & Carroll, J. (2017). Assessing the spatial relationship between fixation and foveal specializations. Vision Research, 132, 53–61. https://doi.org/10.1016/j.visres.2016.05.001

Williams, D. R. (1985). Aliasing in human foveal vision. Vision Research, 25(2), 195–205. https://doi.org/10.1016/0042-6989(85)90113-0

Witten, J. L., Lukyanova, V., & Harmening, W. M. (2024). Sub-cone visual resolution by active, adaptive sampling in the human foveola. eLife, 13, RP98648. https://doi.org/10.7554/eLife.98648

Yarbus, A.L. (1967) Eye Movements and Vision. Plenum Press, New York. http://dx.doi.org/10.1007/978-1-4899-5379-7